International Journal of Pharmaceutics 642 (2023) 123067

Contents lists available at ScienceDirect

International Journal of Pharmaceutics

journal homepage: www.elsevier.com/locate/ijpharm

Harnessing the power of PLA-PEG nanoparticles for Linezolid delivery against methicillin-resistant *Staphylococcus aureus*

Roberto Oliva [a], Giovanna Ginestra [a], Anna Piperno [a], Antonino Mazzaglia [b], Antonia Nostro [a,*], Angela Scala [a,*]

[a] Department of Chemical, Biological, Pharmaceutical and Environmental Sciences, University of Messina, V.le, F. Stagno d'Alcontres, 31, 98166 Messina, Italy
[b] National Council of Research, Institute for the Study of Nanostructured Materials (CNR-ISMN), URT of Messina c/o Department of Chemical, Biological, Pharmaceutical and Environmental Sciences, University of Messina, V.le, F. Stagno d'Alcontres, 31, 98166 Messina, Italy

ARTICLE INFO

Keywords:
Copolymer
CuAAC
Oxazolidinone
MRSA biofilm
Sustained release
Nanoantibiotics

ABSTRACT

This study deals with the development of novel poly(lactic acid)-poly(ethylene glycol) nanoparticles (PLA-PEG NPs) for the efficient and prolonged delivery of Linezolid (LNZ), a synthetic antibacterial agent used against methicillin-resistant *Staphylococcus aureus* (MRSA). A two-step synthetic strategy based on carbodiimide coupling and copper-catalyzed azide-alkyne cycloaddition was first exploited for the conjugation of PLA with PEG. The encapsulation of LNZ into medium-molecular-weight PLA-PEG NPs was carried out by different methods including nanoprecipitation and dialysis. The optimal PLA-PEG@LNZ nanoformulation resulted in 3.5% LNZ payload (15% encapsulation efficiency, with a 10:3 polymer to drug mass ratio) and sustained release kinetics with 65% of entrapped antibiotic released within 80 h. Moreover, the zeta potential values (from −31 to −39 mV) indicated a good stability without agglomeration even after freeze-drying and lyophilization. The PLA-PEG@LNZ NPs exerted antimicrobial activity against a panel of Gram-positive bacteria responsible for human infections, such as *Staphylococcus aureus* including MRSA, *Staphylococcus epidermidis*, *Staphylococcus lugdunensis* and vancomycin-resistant *Enterococcus faecium* (VREfm). Moreover, PLA-PEG@LNZ NPs showed inhibitory activity on both planktonic growth and preformed biofilm of MRSA. The antibacterial activity of LNZ incorporated in polymeric NPs was well preserved and the nanosystem served as an antibiotic enhancer with a potential role in MRSA-associated infections management.

1. Introduction

Linezolid (LNZ) is a synthetic antibacterial agent of the oxazolidinone class active against anaerobic and aerobic Gram-positive and moderately active against a few Gram-negative bacteria (Ager and Gould, 2012). The oxazolidinone mechanism of action differs from all the existing inhibitors of protein synthesis as the inhibition involves the binding of N-formylmethionyl-tRNA (tRNAfMet) to the ribosome, occurring at a very early stage. Specifically, oxazolidinones bind to the A-site pocket of the bacterial 50S ribosomal subunit (without interacting with the 30S subunit) at the peptidyl transferase center (PTC) with consequent inhibition of the initiation complex and translocation of peptidyl-tRNA from A site to P site, thereby halting the translation process (Foti et al., 2021).

Although the leading position of oxazolidinone antibiotics in the current antimicrobial arsenal, only LNZ and Tedizolid (TZL) have been licensed for human use so far. Discovered in 1996 and approved in 2000 for clinical use by the U.S. Food and Drug Administration (Zyvox, Pfizer), LNZ is currently employed for the treatment of surgical or multidrug-resistant (MDR) pulmonary infections caused by vancomycin-resistant *Enterococcus faecium* (VREfm), methicillin-resistant *Staphylococcus aureus* (MRSA), penicillin-resistant pneumococci and also for treating MDR-*Mycobacterium tuberculosis* (Mtb) infections (Bozdogan and Appelbaum, 2004; Foti et al., 2021).

LNZ is currently available in the oral and parenteral dosage forms with a protein-binding of approximately 30 %, a half-life of 5.4 h, and a C_{max} value of about 21 μg/mL, one hour after oral administration (Estes and Derendorf, 2010). The use of 600 mg twice a day for oral Mtb treatment is associated with serious side effects (Choudhary et al., 2022) that are often correlated with prolonged administration.

Based on these premises, there is an urgent need of suitable delivery systems to improve the safety profile of LNZ, to reduce the dose, the

* Corresponding authors.
E-mail addresses: anostro@unime.it (A. Nostro), ascala@unime.it (A. Scala).

https://doi.org/10.1016/j.ijpharm.2023.123067
Received 22 February 2023; Received in revised form 8 May 2023; Accepted 19 May 2023
Available online 29 May 2023

frequency of dosage, the toxicity related to prolonged administration and to improve the dissolution rate that greatly influences the absorption, blood concentration and bioavailability. While nanomedicine tools are currently in use for the design of vaccine carriers (Piperno et al., 2021), nanotechnological approaches to tackle drug-resistant infection diseases are still confined to the laboratory (Labruère et al., 2019). Up to date, only few classes of nanomaterials have been explored as carriers for oxazolidinones, including polymeric nanoparticles (NPs) (Shah et al., 2022) or microspheres (Huang et al., 2017), lipid-polymer hybrid NPs (Guo et al., 2020), mannosylated gelatin NPs (Patil et al., 2020), polymeric nanofibers (Eren Boncu et al., 2020; Tammaro et al., 2015), biocomposite films (Ghataty et al., 2022), nanoemulsions (Choudhary et al., 2022) and cyclodextrin-based inclusion complexes (Hada et al., 2022, Paczkowska-Walendowska et al., 2021). Among these materials, poly(lactic acid) (PLA), poly(lactic-*co*-glycolic acid) (PLGA) and their copolymers with polyethylene glycol (PLA-PEG and PLGA-PEG) emerged as powerful drug carriers for their high entrapment efficiency with sustainable and long-term release, bolstered by their properties of biocompatibility and biodegradability (Scaffaro et al. 2018). The PLA medical use was approved by the Food and Drug Administration for tissue engineering (*e.g.,* design of sutures, bone implants, and screws) and drug/gene delivery purposes (Tyler et al., 2016). Interestingly, the suitable tailoring of PLA matrix by proper chemical functionalization allowed the modulation of the drug release kinetics thereby personalizing therapy for patients with consequent reduction of dosage frequency and mitigation of side effects (Glinka et al., 2021).

Nowadays much attention is paid to amphiphilic copolymer-based nanoformulations for antimicrobial treatment with particular emphasis on nanoantibiotics, namely antibiotics delivered by nanoparticles able to improve physico-chemical properties and pharmacokinetic profile of antimicrobial agents. In this respect, the present study reports, for the first time, the use of a newly synthetized PLA-PEG amphiphilic copolymer as nanocarrier for LNZ delivery with the aim to improve the drug solubility and the dissolution rate, resulting in a prolonged and sustained release of the antibiotic. The amphiphilic PLA-PEG copolymer was synthetized by a proper combination of carbodiimide coupling reaction and copper-catalyzed azide-alkyne cycloaddition (CuAAC) followed by nanoformulation and drug incorporation, leading to PLA-PEG@LNZ NPs. The physicochemical properties of drug-loaded NPs were evaluated in terms of size and zeta potential, pointing out a good colloidal stability without agglomeration even after freeze-drying and lyophilization. Furthermore, drug loading (DL), encapsulation efficiency (EE) and release kinetic were evaluated.

The susceptibility of *Staphylococcus aureus* (*S. aureus*) including MRSA, *Staphylococcus epidermidis* (*S. epidermidis*), *Staphylococcus lugdunensis* (*S. lugdunensis*) and VREfm to PLA-PEG@LNZ NPs was assessed by minimal inhibitory concentration (MIC) and minimal bactericidal concentration (MBC) evaluation. Moreover, MRSA was chosen as the biofilm model because of its clinical relevance as it is involved in various chronic and severe diseases like osteomyelitis, endocarditis, urinary tract infections, implant-associated infections or wound infections. Inhibition of planktonic growth and biofilm of MRSA was estimated after treatment with PLA-PEG@LNZ NPs.

2. Material and methods

2.1. General

Poly(lactic acid) (PLA, 10.000–17.000 Da), methoxypolyethylene glycol azide (mPEG-N_3, 2.000 Da), N-(3-dimethylaminopropyl)-N′-ethylcarbodiimide hydrochloride (EDCI), 1-hydroxybenzotriazole hydrate (HOBt), solvents and other reagents were purchased from Merck (Italy). ^{1}H NMR spectra were recorded on a Varian 500 MHz spectrometer at room temperature (r.t. 25 °C). UV/Vis spectra were registered on a Agilent model 8453 diode array spectrophotometer using 1 and 0.2 cm path length quartz cells, at 25 °C using a thermostatic bath. Hydrodynamic diameter (D_H) or size and width of distribution (polydispersity index, PDI) were determined in ultrapure water by photon correlation spectroscopy (PCS) by a Zetasizer Nano ZS (Malvern Instrument, Malvern, U.K.) at 25 °C. The measurements were performed at 173° angle vs. the incident beam at 25 ± 1 °C for each aqueous dispersion. The deconvolution of the correlation curve to an intensity size distribution was obtained using a non-negative least-squares algorithm. The ζ-potential values were measured using a Zetasizer Nano ZS Malvern Instrument equipped with a He − Ne laser at a power P = 4.0 mW and λ = 633 nm. Results are reported as the mean of three separate measurements on three different batches ± the standard deviation (SD).

2.2. Synthesis of PLA-PEG copolymer

2.2.1. Synthesis of PLA-alkyne

PLA (**1**) (0.2 g, 1.43×10^{-5} mol) was dissolved in anhydrous dichloromethane (DCM, 10 mL) under nitrogen atmosphere, followed by the addition of EDCI (5 equiv) and HOBt (5 equiv). After 30 min, propargylamine (**2**) (5 equiv) was added and the reaction mixture was stirred under nitrogen atmosphere for 24 h at r.t. The organic solution was washed with distilled water three times, the organic phases were combined and then dried over anhydrous Na_2SO_4. The product PLA-alkyne (**3**) was isolated by evaporation of the solvent under vacuum as a white solid (0.17 g). ^{1}H NMR (500 MHz, $CDCl_3$, δ): 6.6–6.4 (br s, NH), 5.3–5.1 (m, $[CH]_n$), 4.9–5.0 (m, $\underline{CH}$-$COOH_{unreacted}$), 4.3 (q, $\underline{CH}$-OH), 4.0–4.1 (m, 2H, NH$\underline{CH_2}$), 2.2 (m, 1H, C≡$\underline{CH}$), 1.6–1.4 (m, $[CH_3]_n$). M_n ^{NMR} 11.592 Da.

2.2.2. Synthesis of PLA-PEG

PLA-alkyne (**3**) (0.15 g, 1.04×10^{-5} mol) was dissolved in anhydrous dimethylformamide (DMF, 3 mL). Then, mPEG-N_3 (**4**) (1 equiv), $CuSO_4$ (2 equiv) and sodium ascorbate (4 equiv) were added under nitrogen atmosphere. The reaction mixture was stirred under inert atmosphere for 48 h at r.t. Water was added till the solution became opalescent. The suspension was centrifuged three times (13000 rpm, 20 min); the solid residue was lyophilized to obtain the final product PLA-PEG (**5**) as a white solid (0.11 g). ^{1}H NMR (500 MHz, $CDCl_3$, δ): selected peaks 7.3 (s, H-$5_{triazole}$), 6.6–6.4 (br s, NH), 5.2–5.1 (m, $[CH]_n$), 4.9–5.0 (m, $\underline{CH}$-$COOH_{unreacted}$), 4.35 (q, $\underline{CH}$-OH), 3.8–3.6 (s, $[CH_2CH_2O]$), 3.3 (s, CH_3O), 1.6–1.4 (m, $[CH_3]_n$). M_n ^{NMR} 13.044 Da. From NMR analysis, the content of PEG grafted on PLA was estimated to be ≈ 11 w/w %.

2.3. Preparation of PLA–PEG@LNZ NPs

2.3.1. Nanoprecipitation with Acetone/H_2O

PLA-PEG@LNZ NPs were prepared by nanoprecipitation method (Fig. 1) using acetone as organic phase and a polymer:drug mass ratio of 10:3. LNZ (9 mg) and PLA-PEG (30 mg) were dissolved in 6 mL of acetone. This solution was added dropwise to 12 mL of stirring ultrapure water. After 24 h, once acetone was evaporated, 300 μL of the resulting suspension of NPs were diluted to 1 mL with water and used for the revelation of hydrodynamic diameter and surface charge of the freshly formulated NPs. The suspension was centrifuged at 13000 rpm for 10 min. The residue was freeze-dried yielding PLA-PEG@LNZ NPs as a white powder.

2.3.2. Nanoprecipitation with THF/H_2O

PLA-PEG@LNZ NPs were prepared by nanoprecipitation method (Fig. 1) using THF as organic phase and a polymer:drug mass ratio of 10:3. LNZ (9 mg) and PLA-PEG (30 mg) were dissolved in 3 mL of THF. The solution was added dropwise to 30 mL of stirring ultrapure water. After stirring for 4 h, THF was evaporated under vacuum and 450 μL of the obtained suspension were diluted up to 1.5 mL with water for measure the size and surface charge of the freshly formulated NPs. The suspension is centrifuged at 13000 rpm for 10 min and the residue was freeze-dried yielding PLA-PEG@LNZ NPs as a white powder.

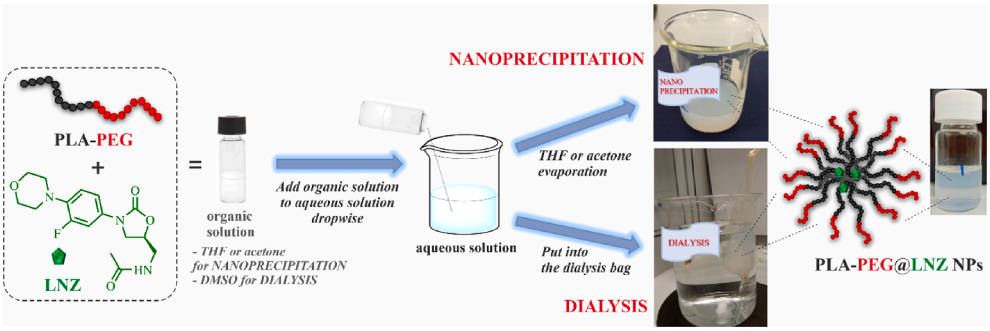

Fig. 1. Schematic illustration of the PLA-PEG@LNZ NPs preparation by nanoprecipitation and dialysis methods.

2.3.3. Dialysis

PLA-PEG@LNZ NPs were prepared by dialysis method (Fig. 1) at 10:3 polymer:drug mass ratio. LNZ (9 mg) and PLA-PEG (30 mg) were dissolved in 1 mL of DMSO. After a brief sonication, the organic solution was added dropwise to 20 mL of stirring ultrapure water with the formation of a suspension. After 4 h of stirring, the suspension was transferred into a dialysis membrane (3.5–5 kDa cut-off) previously conditioned in water for 10 min. The sealed dialysis tube was immersed in 500 mL of ultrapure water and kept under gentle stirring. The entire volume of water was replaced after 3 h, after 15 h and 30 min, after 19 h and 30 min. The final suspension was lyophilized, yielding PLA-PEG@LNZ NPs as a white powder. Similarly, "empty" PLA-PEG NPs were prepared with the same method, without adding the drug and used as controls.

2.4. Characterization of PLA-PEG@LNZ NPs

2.4.1. Drug loading

The drug content in the NPs and the loading efficiency were determined by UV–Vis spectroscopy. Briefly, a weighted amount of PLA-PEG@LNZ NPs was solubilized in DMSO and the UV–Vis spectrum was recorded. The amount of encapsulated LNZ was calculated at the wavelength of 262 nm. A calibration curve for LNZ in DMSO was previously constructed in the concentration range 25–150 μg/mL. On the basis of optical absorbance data and molar extinction coefficient ($\varepsilon \cong 17758\ M^{-1}\ cm^{-1}$), drug loading (DL) and encapsulation efficiency (EE) were calculated using the following equations:

$$-DL\ (\%) = (\text{Drug weight in the NPs/Weight of the drug-loaded NPs}) \times 100$$

$$-EE\ (\%) = (\text{Drug weight in the NPs/Weight of drug used in the formulation}) \times 100$$

2.4.2. Size and zeta potential (ζ)

Measurements were carried out on both the freshly prepared NPs and the lyophilized NPs after reconstitution. The lyophilized white solid was resuspended in ultrapure water (1 mg/mL), sonicated for 15 min and then diluted (final concentration: 0.3 mg/mL) for DLS and ζ-potential measurements.

2.4.3. Release studies

To study the drug release, 0.91 mg of PLA-PEG@LNZ NPs (containing 32 μg LNZ) were dispersed in 1 mL of PBS (0.01 M, pH 7.4), sonicated for 15 min and transferred into a dialysis tube (MWCO 3.5–5 kDa, Spectra/Por®). Dialysis was performed against 5 mL PBS at 37 °C. At fixed times (4 h, 24 h, 32 h, 48 h, 56 h, 80 h), 1 mL of the release medium was withdrawn, replaced with an equal volume of fresh buffer, and analysed by UV–Vis spectroscopy to quantify the released LNZ. A calibration curve of LNZ in PBS was previously constructed in the concentration range 0.34–25 μg/mL ($\varepsilon \cong 18486\ M^{-1}\ cm^{-1}$). Then, all the release medium solutions and the internal bag solution were lyophilized, re-disperded in DMSO and analysed by UV–Vis spectroscopy to confirm the data. Free LNZ in PBS was dialyzed at the same concentration as the drug-loaded NPs (*i.e.,* 32 μg/mL) in similar experimental conditions as control.

2.5. Microbiological studies

2.5.1. Minimal inhibitory concentration and minimal bactericidal concentration

The microorganisms used in this study were *S. aureus* ATCC 6538, MRSA ATCC 43300, *S. epidermidis* ATCC 35984, *S. lugdunensis* DSM 4804 and VREfm DSM 17050. Minimal inhibitory concentration (MIC) and minimal bactericidal concentration (MBC) of the PLA-PEG@LNZ NPs (containing 32 μg LNZ in 914 μg of NPs, based on DL value), LNZ and empty PLA-PEG NPs were performed according to the guidelines of the Clinical and Laboratory Standards Institute (CLSI), CLSI (2018) with some modifications. The samples were twofold diluted in 96-well round-bottomed using cation-adjusted Muller-Hinton broth (CAMHB, Oxoid) and overnight bacterial cultures were inoculated to yield a final concentration of 5×10^5 CFU/mL. After incubation at 37 °C for 24 h, the MBC was determined by seeding 20 μL from all clear wells onto Muller-Hinton agar (MHA) and incubated at 37 °C for 24 to 48 h. The MBC was defined as the lowest concentration which killed 99.9% of the inoculum. The data from at least three replicates were evaluated and modal results were calculated.

2.5.2. Effect of PLA-PEG@LNZ NPs on planktonic cells

Overnight culture of MRSA ATCC 43300 grown in CAMHB was adjusted to a concentration of 1×10^6 CFU/mL, approximatively. The standardized inoculum was dispensed in tubes containing PLA-PEG@LNZ NPs at MIC, 2 × MIC, 4 × MIC [corresponding to a LNZ content of 8, 16 and 32 μg/mL, respectively, and a LNZ release of about 25% in 24 h, 46% in 48 h, and 60% in 72 h (see release data)], free LNZ at MIC, 2 × MIC, 4 × MIC (corresponding to 2, 4 and 8 μg/mL, respectively), or empty PLA-PEG NPs (the latter were tested at the same polymer concentration used for testing the drug-loaded NPs). The tubes were incubated at 37 °C with shaking (100 rev/min) and after 2, 4, 6, 24, 48, 72 h the samples were serially diluted in PBS and were plated onto MHA to determine total cell number. The plates were then incubated at 37 °C for 24 h up to 48 h, CFU were counted and time kill plots were constructed. All determinations were performed in triplicate including the growth control.

2.5.3. Effect of PLA-PEG@LNZ NPs on preformed biofilm

Effect of PLA-PEG@LNZ NPs on preformed biofilm was estimated as previously reported (Nostro et al. 2007 and 2009). Overnight cultures of MRSA ATCC 43300 in Tryptic Soy Broth (TSB) + 1% glucose (TSBG) were adjusted to 1×10^6 CFU/mL and 100 μL were added individually to each well of a polystyrene flat bottomed 96-microtitre plate. The plates were incubated at 37 °C for 24 h. After incubation, the supernatant was

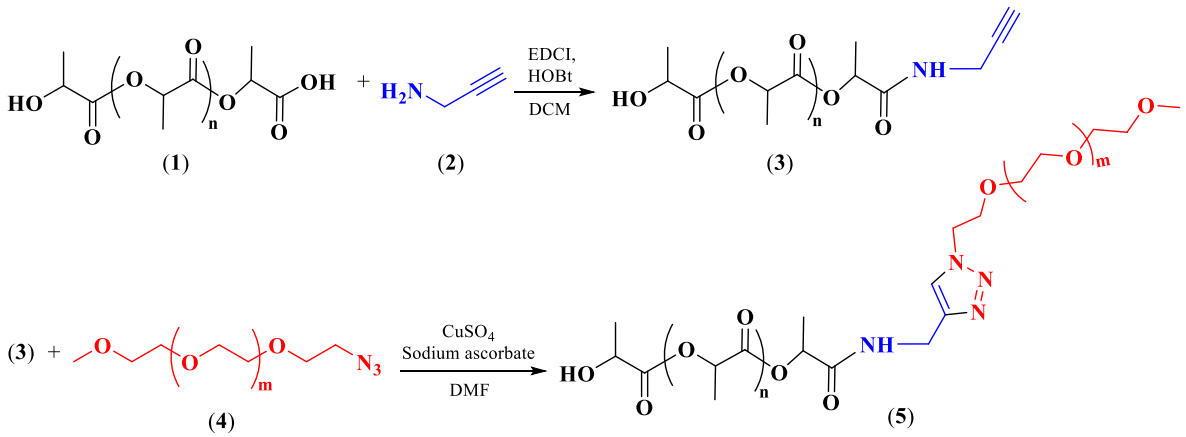

Scheme 1. Two-step synthesis of the copolymer PLA-PEG (**5**).

removed and biofilms were carefully washed twice with sterile PBS. Biofilms were treated with 100 μL of PLA-PEG@LNZ NPs at 2 × MIC, 4 × MIC, free LNZ at 2 × MIC, 4 × MIC, empty PLA-PEG NPs or CAMHB (control) for 24 h at 37 °C.

To determine whether the PLA-PEG@LNZ NPs treatment inhibited the growth in biofilm supernatant, the optical density (OD_{492}) was measured at time 0 (T0) and after incubation for 24 h. The growth inhibition in biofilm supernatant was detected when there was no observable bacterial growth in the wells, confirmed by no increase in optical density compared with the initial reading. To verify the activity on biofilm biomass and cell viability, the supernatant was removed and biofilms were washed twice with PBS before being:

i) dried, stained for 1 min with 0.1% safranin and resuspended in 30% (v/v) acetic acid for OD_{492} evaluation;
ii) resuspended in 100 μL of PBS and scraped with sterile pipette tips for evaluation of the bacterial load (CFU) by plating serial dilutions onto MHA.

2.5.4. Effect of PLA-PEG@LNZ NPs on biofilm re-growth

Effect of PLA-PEG@LNZ NPs on biofilm re-growth was estimated as previously reported (Nostro et al. 2009) with some modifications. The experiment was designed in two steps. First, the influence of a treatment with PLA-PEG@LNZ NPs 4 × MIC (corresponding to a LNZ content of 32 μg/mL and a LNZ release < 25 % in 12 h) or free LNZ at 4 × MIC (corresponding to 8 μg/mL) for 12 h on growth of biofilm supernatant and viable cells of MRSA ATCC 43300 was evaluated. Subsequently, to determine whether PLA-PEG@LNZ NPs and free LNZ treatment prevented the re-growth of bacteria embedded in the biofilm, the medium was removed, the biofilm was washed with PBS and fresh CAMHB was added. Plates were re-incubated at 37 °C overnight and the biofilm supernatant and viable cells were evaluated as described above.

2.5.5. Statistical analysis

Results were expressed as the mean ± standard deviation from three experiments. Student's *t*-test and ANOVA test were used to determine significant differences between the treated samples compared with T0 and between the samples treated with PLA-PEG@LNZ NPs and free LNZ. The results with a *p*-value < 0.05 were considered statistically significant.

3. Results and discussion

3.1. Chemistry

The conjugation of PLA with PEG was achieved using a suitable combination of two typical coupling reactions such as the carbodiimide-mediated coupling and the copper-catalyzed azide-alkyne cycloaddition (CuAAC). They are powerful tools in polymer organic chemistry due to their high conversion efficiency, mild reaction conditions, biocompatibility, with no side-products (Scala et al., 2018a and 2018b; Liénard et al., 2020; Torcasio et al., 2022). Specifically, the carboxylic group of PLA (**1**) was activated by EDCI/HOBt for the subsequent reaction with propargylamine (**2**) leading to PLA-alkyne (**3**). The latter was coupled with methoxypolyethylene glycol azide (**4**) by CuAAC to obtain the final PLA-PEG copolymer (**5**) (Scheme 1).

The structure of both the intermediate (**3**) and the final product (**5**) was confirmed by ^{1}H NMR analysis (Fig. S1). The characteristic signals of lactoyl repeating units were clearly visible at 1.5 ppm (CH_3) and 5.2 ppm (CH) in both ^{1}H NMR spectra, together with the resonances at 4.1 ppm (CH_2 protons of propargylamide moiety, shifted from 3.5 ppm of starting propargylamine) and the amidic NH signals (6.6–6.4 ppm). The typical triazole H-5 proton resonance at 7.3 ppm and the signal at 3.7 ppm (–CH_2CH_2O- units of PEG) attested for the conversion of (**3**) to (**5**), confirming the successful connection of the hydrophilic PEG with the hydrophobic PLA.

3.2. Nanoformulation

The nanoformulation of PLA-PEG and the drug encapsulation were carried out using two different methods, *i.e.* nanoprecipitation (both in THF and in acetone) and dialysis, at 10:3 polymer to drug mass ratio, with the aim to explore different techniques for PLA-PEG@LNZ NPs preparation.

The nanoantibiotic prepared by dialysis was selected for the biological investigation based on the highest drug loading (DL) value obtained. Specifically, DL measured by UV–Vis spectrophotometry resulted 0.6 % and 0.9 % for the nanoprecipitation in acetone and in THF, respectively, and 3.5 % for the dialysis formulation; the encapsulation efficiency (EE) was estimated to be 2.6, 4.1 and 15 %, respectively (Table 1). All the samples owned a monomodal particle size distribution, either before ("freshly prepared") and after centrifugation and freeze-drying, suggesting that the D_H value was slightly influenced by lyophilization and reconstitution (Table 1). The ζ-potential attested for negatively charged NPs, as typically found for aliphatic polyester NPs, with a net negative charge ranging from −31 to −39 mV (Table 1), indicating a good colloidal stability.

^{1}H NMR measurements were further employed to investigate the structure of PLA-PEG@LNZ NPs and to confirm the drug incorporation (Fig. 2). It's well known that amphiphilic PLA-PEG copolymers are able to self-assemble in water exposing the hydrophilic portion toward the aqueous solution whereas the hydrophobic moiety constitutes the *core* incorporating hydrophobic drugs. As expected (Fazio et al., 2015), the characteristic peak of PEG at 3.7 ppm was the only one detected in D_2O

Table 1
Overall properties of NPs: mean Hydrodynamic Diameter (D_H), Polydispersity Index (PDI) and ζ-potential (ζ) in ultrapure water; Drug Loading (DL) and Encapsulation Efficiency (EE). Size distributions and ζ-potential are reported in Fig. S2, Supporting Information.

Sample	D_H (nm ± SD) (%)[a]	PDI	ζ (mV ± SD)	DL (%)	EE (%)
PLA-PEG@LNZ NPs (nanoprecipitation $_{acetone}$)	263 ± 98[b]	0.15	−31 ± 4[b]	0.6%	2.6%
	[489 ± 86 (92) 131 ± 16 (8)][c]	0.05 0.05	[-39.5 ± 5.4][c]		
PLA-PEG@LNZ NPs (nanoprecipitation $_{THF}$)	206 ± 72[b]	0.1	−34 ± 6[b]	0.9%	4.1%
	[264 ± 96][c]	0.15	[-38 ± 6][c]		
PLA-PEG@LNZ NPs (dialysis)	332 ± 132[b]	0.2	−34.6 ± 6.4[b]	3.5%	15%
	[295 ± 48][c]	n.d.	[-37.3 ± 6.6][c]		
Empty PLA-PEG NPs	180 ± 53[b]	0.1	−38 ± 8.5[b]	–	–

[a] Mean size with corresponding intensity % distribution. [b]Each DLS and ζ-potential measurement was carried out on "freshly prepared" NPs in triplicate at 25 °C (SD was calculated on the three different batches). [c]The values in bracket referred to lyophilized and reconstituted NPs.

(Fig. 2, blue line) indicating that the water-soluble PEG backbone constitutes the outer shell of the polymeric NPs, while PLA and LNZ peaks disappeared in D_2O, confirming that the PLA-based hydrophobic *core* is responsible for drug incorporation. However, all the peaks of PEG, PLA and LNZ are visible in DMSO-d_6 (Fig. 2, red line), the solvent in which the system is typically disassembled, according to literature (Fazio et al., 2015).

3.3. Release studies

The drug release kinetics of PLA-PEG@LNZ NPs and free LNZ were studied in PBS using the dialysis bag method. The cumulative percentage release and release rate of LNZ were plotted in Fig. 3. Free LNZ had a very quick release up to 56% within the initial 4 h, as expected, due to the fast diffusion of the drug across the dialysis membrane and a complete drug release (97%) was observed within 72 h. In contrast, the drug release from PLA-PEG@LNZ NPs was sustained and controlled and approximately 65% of drug release was observed within 80 h; overall the release rate of incorporated LNZ was lower than that of free drug under the same concentration and experimental conditions. From our experimental results, we assumed that about 50% of drug was released from PLA-PEG@LNZ NPs within 48–56 h. Specifically, about 25% of LNZ was released in the first 24 h, reaching 39% in 32 h, 46% in 48 h, 57% in 56 h and about 65% of the payload was released by the end of the experiment (*i.e.,* 80 h). During the burst release phase, about 13% of LNZ was released in the first 4 h, whereas a gradual and sustained release of the drug was observed over 80 h. The most rapid drug release in the first hours was mainly associated with the diffusion of drug from the surface of the NPs in the release medium, prior to the onset of polymer erosion-mediated drug release. Since LNZ has a certain solubility in water, it

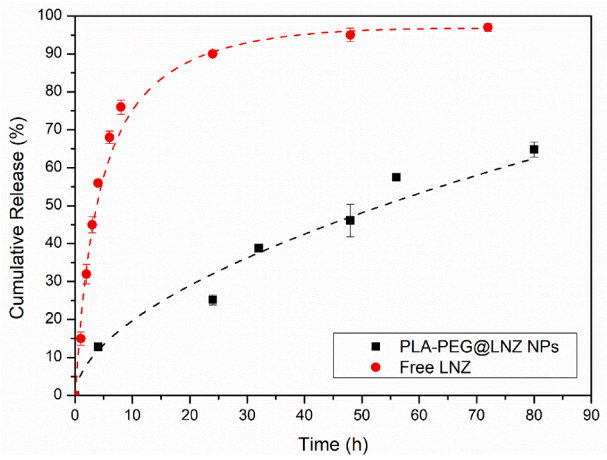

Fig. 3. Cumulative percentage release of LNZ as free drug (●) and from PLA-PEG@LNZ NPs (■) as a function of time, assessed by dialysis in PBS (pH 7.4) at 37 °C. Data are reported as the mean ± SD ($n = 3$).

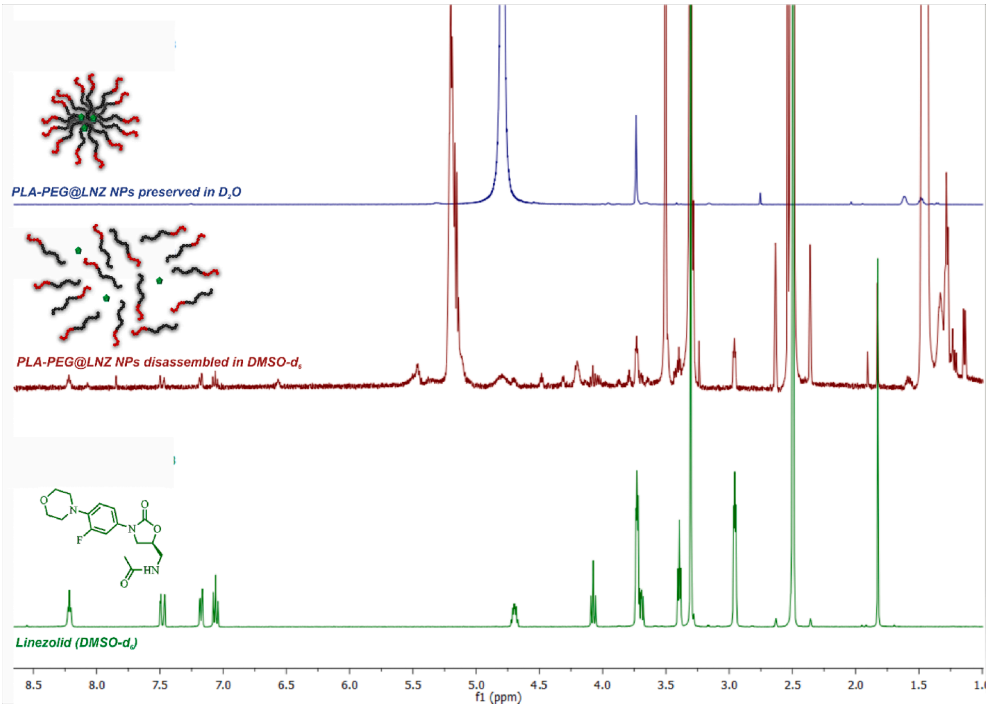

Fig. 2. ^{1}H NMR of PLA-PEG@LNZ NPs in D_2O (blue) and in DMSO-d_6 (red). The ^{1}H NMR of free LNZ in DMSO-d_6 (green) is also reported for comparison.

tends to diffuse into the outer aqueous phase during the NPs preparation, resulting in its encapsulation in the outer layer or attachment to the surface of the NPs (Huang et al., 2017), in well agreement with other antibiotics delivered by polymeric NPs (*i.e.,* Amikacin) (Glinka et al., 2021). Thus, the most rapid release of LNZ in the first hours was associated with the presence of molecules on or trapped near the surface of the PLA-PEG NPs, whereas the slower drug release in subsequent hours was due to the presence of drug molecules in the deeper layers of the NPs, together with polymer erosion and hydrolytic bulk degradation and/or swelling. Overall, we would like to point out that a rapid drug release followed by a prolonged and sustained trend is highly desiderable for nanomaterials with antimicrobial applications.

3.4. Microbiological studies

The MIC values of LNZ were between 1 and 2 μg/mL for the studied microorganisms with greater activity (1 μg/mL) toward *S. epidermidis* and *S. lugdunensis* compared with *S. aureus* (Table 2). According with literature data, MIC values of LNZ is similar for methicillin-susceptible *S. aureus* (MSSA) and MRSA strains (Karlowsky et al., 2017). Although the MIC values of PLA-PEG@LNZ NPs seemed increased compared to free LNZ (*i.e.,* 4–8 *vs* 1–2 μg / mL), they should be evaluated taking in account the release profile (Fig. 3) and specifically considering that only about 25% of LNZ was released from NPs in the first 24 h. Therefore, the activity of LNZ embedded in NPs was preserved.

The results were confirmed by the effect on planktonic growth of MRSA ATCC 43300 registered till 72 h (Fig. 4). Free LNZ was bacteriostatic at 2 μg/mL (*i.e.,* the MIC for this strain) only up to 24 h with a horizontal time-kill plot (orange line) after which it did not prevent bacterial growth but a regrowth started, likely due to the fast release of free drug at 24 h (see Fig. 3).

A reduction of bacterial load was detected at higher concentrations of free LNZ (*i.e.,* 4 and 8 μg/mL, namely LNZ 2 × MIC and LNZ 4 × MIC, respectively). In fact, at concentration of LNZ 4 × MIC (violet line), bacterial count declined up to 24 h from baseline 1.2×10^6 CFU/mL to 4.8×10^3 CFU/mL (2.4 Log decrease). At the end of this phase, bacterial cells entered in a persisting phase with a small proportion of viable bacteria survived beyond 48 h (2×10^3 CFU/mL; 2.78 Log decrease) that further reduced to 4.5×10^2 CFU/mL (3.43 Log decrease) at 72 h. A similar trend was observed for LNZ 2 × MIC (light blue line). The growth control reached a maximum of $\sim 10^{10}$ CFU/mL (Fig. 4).

It is noteworthy that the drug incorporated into the NPs × MIC (green line) was significantly effective in reducing the bacterial load from baseline 1.2×10^6 to $2.3–1 \times 10^4$ CFU/mL (1.72–2.08 Log decrease) over 24–48 h, followed by a reduction to 3×10^3 CFU/mL (2.61 Log decrease) at 72 h, differently from free LNZ at the MIC (orange line). PLA-PEG@LNZ NPs 4 × MIC (blue line) determined the reduction of bacterial cells to 1.6×10^4 CFU/mL (1.88 Log decrease) at 24 h followed by a decrease to 8×10^2 CFU/mL (3.18 Log decrease) at 48 h and 4.8×10^2 CFU/mL (3.39 Log decrease) at 72 h, compared to control untreated. A similar trend was also observed for PLA-PEG@LNZ NPs 2 × MIC (red line).

Altogether these results confirmed that the native antimicrobial effect of the drug was preserved even after incorporation and pointed out that the main advantage of our nanosystem is the prolonged activity of

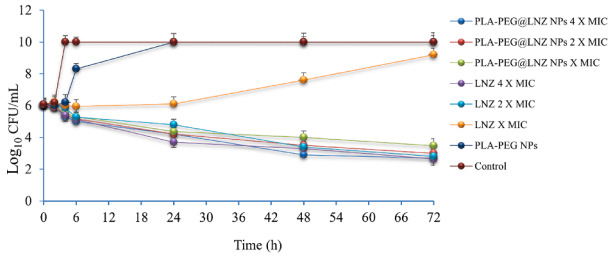

Fig. 4. Effects of PLA-PEG@LNZ NPs, free LNZ and empty PLA-PEG NPs on planktonic growth of MRSA ATCC 43300. All data are presented as mean ± SD. Free LNZ at MIC, 2 × MIC, and 4 × MIC correspond to 2, 4, 8 μg/mL, respectively. PLA-PEG@LNZ NPs at MIC, 2 × MIC, 4 × MIC correspond to a LNZ content of 8, 16, 32 μg/mL. About 25% of drug was released in 24 h, 46% in 48 h and 60 % in 72 h (see release data). Significant difference ($p < 0.01$, confidence interval: 99%) was detected between PLA-PEG@LNZ NPs and free LNZ at the MIC (green and orange lines, respectively). No significant difference ($p > 0.05$) was found between PLA-PEG@LNZ NPs and free LNZ at concentrations 4 × MIC and 2 × MIC.

LNZ loaded into PLA-PEG@LNZ NPs × MIC till 72 h, compared to free LNZ × MIC that is active only till 24 h. Although the antimicrobial activity of free drug (2 × MIC and 4 × MIC) and drug-loaded NPs appeared to be similar in the time kill plots (Fig. 4), only PLA-PEG@LNZ NPs 4 × MIC determined a reduction of bacterial load of 3 Log in CFU/mL as early as 48 h.

MRSA is a major public health problem all over the world and represents a therapeutic problem for both antibiotic resistance and ability to adhere to different surfaces and form thick multilayered biofilm. Once firmly established, a biofilm is very difficult to eradicate because the bacteria embedded in a self-produced matrix exhibit poor susceptibility to conventional antimicrobial treatment. The relatively poor efficacy of LNZ in eradicating established *S. aureus* biofilm is well demonstrated in literature (Cafiso et al., 2010; Sivori et al., 2022). Abad et al. reported the inefficiency of LZN against biofilm-embedded *S. aureus* with minimum biofilm eradication concentrations (MBECs) values > 2000 mg/L for three different strains, including one reference strain (6850) and two clinical isolates implicated in chronic bone and joint infections (BJIs) (Abad et al., 2019) and Curtin et al. reported that more than 72 h is required for LNZ (2000 mg/L) to achieve eradication of *S. epidermidis* biofilms (Curtin et al., 2003). With that in mind, the aim of our study was also to improve the activity of LNZ against MRSA biofilm. The effect of PLA-PEG@LNZ NP and free LNZ on 24 h biofilm was determined as biofilm retention both in terms of biomass (optical density) and cells viability (CFU/mL). The results reported in Fig. 5 demonstrated that PLA-PEG@LNZ NPs 4 × MIC and 2 × MIC reduced the biomass of 38% and 27%, respectively, compared to the control (biofilm at T0). Conversely, a negligible biomass reduction (~2%) was observed after 24 h treatment with free LNZ at two concentrations (*i.e.,* 4 × MIC and 2 × MIC).

Regarding biofilm viability, PLA-PEG@LNZ NPs 4 × MIC determined the reduction of CFU/mL by 64%, from baseline 1.6×10^7 to 5.8×10^6 CFU/mL after 24 h treatment (Fig. 6); halving the dose (PLA-PEG@LNZ NPs 2 × MIC) the effect was bacteriostatic, whereas free LNZ, empty NPs

Table 2
Antibacterial activity of free LNZ, PLA-PEG@LNZ NPs expressed as LNZ concentration (μg/mL) and empty PLA-PEG NPs.

Samples	*S. aureus* ATCC 6538		MRSA ATCC 43300		*S. epidermidis* ATCC 35984		*S. lugdunensis* DSM 4804		VREfm DSM 17050	
	MIC	MBC	MIC	MBC	MIC	MBC	MIC	MBC	MIC	MBC
LNZ	2	16	2	16	1	16	1	16	2	16
PLA-PEG@LNZ NPs	8	>16	8	>16	4	>16	4	>16	>16	>16
PLA-PEG NPs	-[a]	-	-	-	-	-	-	-	-	-

[a]No activity was detected for empty PLA-PEG NPs at the highest tested concentration.

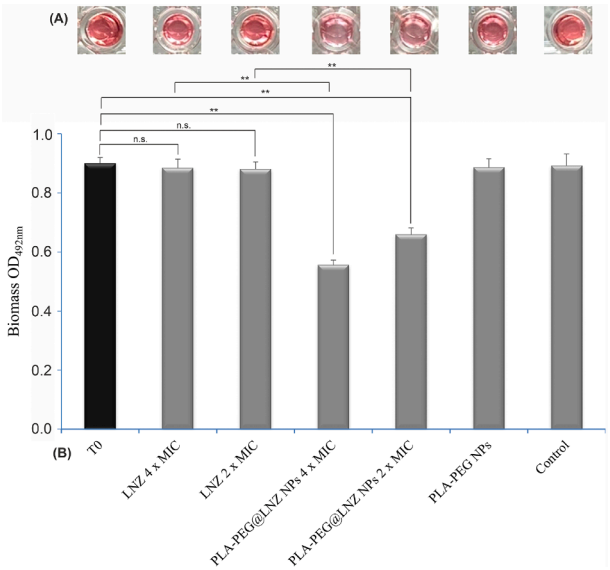

Fig. 5. Efficacy of free LNZ, PLA-PEG@LNZ NPs and empty PLA-PEG NPs at different concentrations on biofilm biomass of MRSA ATCC 43300. (**A**) Representative photographs of biofilm biomass. (**B**) Quantitative analysis of biofilm biomass. Black histogram: biofilm at time = 0 (T0) without treatment. Grey histograms: biofilm after treatment with free LNZ, PLA-PEG@LNZ NPs, empty PLA-PEG NPs and CAMHB (control) for 24 h. The results are shown as the mean ± standard deviation of the values obtained from three independent experiments. Statistical significance of comparison between each treatment and T0 and between PLA-PEG@LNZ NPs and free LNZ was calculated. ** *p*-value < 0.01 (confidence interval: 99%); n.s., not significant *p*-value > 0.05.

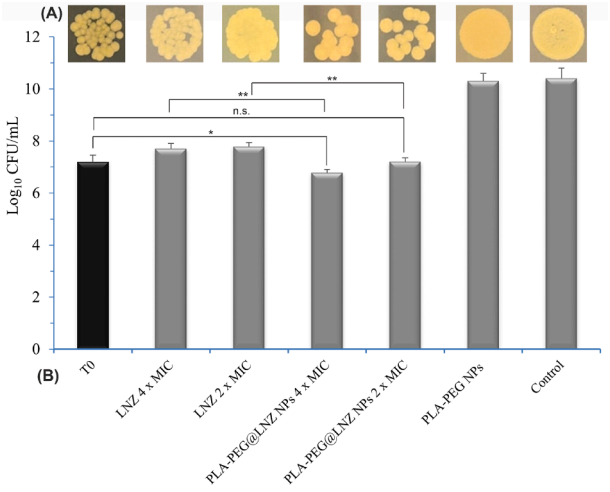

Fig. 6. Effect of free LNZ, PLA-PEG@LNZ NPs and empty PLA-PEG NPs at different concentrations on the biofilm viable cells of MRSA ATCC 43300 after 24 h-treatment (**A**) Representative photographs of biofilm viable cells. (**B**) Quantitative analysis of biofilm viable cells. Black histogram: biofilm at time = 0 (T0) without treatment. Grey histograms: biofilm after treatment with free LNZ, PLA-PEG@LNZ NPs, empty PLA-PEG NPs and CAMHB (control) for 24 h. The results are shown as the mean ± standard deviation of the values obtained from three independent experiments. Statistical significance of comparison between each treatment and T0 and between PLA-PEG@LNZ NPs and free LNZ was calculated. * *p*-value < 0.05 (confidence interval: 95%); ** *p*-value < 0.01 (confidence interval: 99%); n.s., not significant *p*-value > 0.05.

and control revealed an increase of CFU/mL (Fig. 6). These data were consistent with the activity reported in Table S1 (Supporting Information) documenting the ability of PLA-PEG@LNZ NPs to inhibit the growth in biofilm supernatant compared to free LNZ.

The current results documented that PLA-PEG@LNZ NPs showed inhibitory activity on biofilm-embedded MRSA in terms of biomass and cell viability; conversely, a negligible effect on optical density reduction and even a revival of bacterial biofilm growth was observed with free LNZ. Moreover, we would like to point out that the effect of LNZ-loaded NPs 4 × MIC should be considered taking in account that NPs released only about 25% of the loaded drug during 24 h which is the experimental time of biofilm evaluation.

The anti-biofilm activity of PLA-PEG@LNZ NPs could be attributed to the ability of the NPs to diffuse through the water channels (pores) of the biofilm (Kalishwaralal et al., 2010) and to improve the physical contact between antibiotic and bacterial cells. Indeed, literature data reported that anionic NPs are able to rapidly reach deepest bacteria in biofilms and sustainably deliver the incorporated antibiotic during the time (Da Costa et al., 2021).

However, the washing of biofilm after 12 h-treatment caused loss of activity with bacterial re-growth, as demonstrated after re-incubation in broth at 37 °C for 24 h (Figure S3 and Table S2 Supporting Information). These findings can be supported by a previous investigation (Da Costa et al. 2021) correlating the surface charge of PLA NPs with their retention capacity in biofilms and related efficacy. Specifically, negatively charged NPs homogeneously migrated through the whole *S. aureus* biofilms and sustainably deliver antibiotic but they were easily washed out; conversely positively charged NPs were shown to adhere and were greatly retained in the biofilm, limiting their washout and maintaining efficacy.

4. Conclusions

In summary, we demonstrated that nanotechnology might provide novel opportunities to re-explore the antimicrobial efficacy of known antibiotics such as LNZ, overcoming the limits of the standard administration. We have designed and produced novel PLA-PEG NPs incorporating LNZ that preserved the antimicrobial activity of the drug providing a gradual and sustained release over the time. The amphiphilic copolymer was synthetized by a proper combination of coupling reactions, such as the carbodiimide-mediated coupling and the copper-catalyzed azide–alkyne cycloaddition, followed by nanoformulation and drug incorporation. LNZ-loaded PLA-PEG NPs turned out to serve as antibiotic enhancer with a potential role in MRSA-associated infections. Interestingly, the gradual and sustained release of LNZ from our polymeric NPs provided a long-lasting supplier of drug that might keep concentrations above MICs allowing the maximal effect of time-dependent antibiotics. Harnessing the power of PLA-PEG NPs for LNZ delivery turned out to be a strategic tool for treating bacterial infections in a biofilm context (*i.e.,* for MRSA infections management) considering the recalcitrance of biofilms toward conventional antibiotic therapies. In perspective, our findings open the way for further investigations on LNZ-loaded PLA-PEG NPs including the binding with proteins, the drug half-life, the charge-reversed PLA NPs for biofilm-associated treatment (*i.e.*, poly-L-lysine surface-decorated PLA NPs), the dual antimicrobial drug-loaded nanoformulations able to synergistically enhances the efficacy of LNZ.

CRediT authorship contribution statement

Roberto Oliva: Investigation, Writing – review & editing. **Giovanna Ginestra:** Investigation, Writing – review & editing. **Anna Piperno:** Investigation, Writing – review & editing. **Antonino Mazzaglia:** Investigation, Writing – review & editing. **Antonia Nostro:** Validation, Writing – original draft, Visualization, Supervision, Writing – review & editing. **Angela Scala:** Conceptualization, Methodology, Validation, Writing – original draft, Visualization, Supervision, Project administration, Funding acquisition, Writing – review & editing.

Declaration of Competing Interest

The authors declare that they have no known competing financial interests or personal relationships that could have appeared to influence the work reported in this paper.

Data availability

Data will be made available on request.

Acknowledgements

This work was partially supported by the grant "FFABR, Italy, University of Messina, Finanziamento Attività di Base della Ricerca di Ateneo FFABR Unime 2021_SCALA_ANGELA"

Appendix A. Supplementary data

Supplementary data to this article can be found online at https://doi.org/10.1016/j.ijpharm.2023.123067.

References

Abad, L., V. Tafani, V., Tasse, J., Josse, J., Chidiac, C., Lustig, S., Ferry, T., Diot, A., Laurent, F., Valour, F., 2019. Evaluation of the ability of linezolid and tedizolid to eradicate intraosteoblastic and biofilm-embedded *Staphylococcus aureus* in the bone and joint infection setting. J. Antimicrob. Chemother. 74, 625–632. https://doi.org/10.1093/jac/dky473. PMID: 30517641.

Ager, S., Gould, K., 2012. Clinical update on linezolid in the treatment of Gram-positive bacterial infections. Infect. Drug Resist. 5, 87–102. https://doi.org/10.2147/IDR.S25890.

Bozdogan, B., Appelbaum, P.C., 2004. Oxazolidinones: activity, mode of action, and mechanism of resistance. Int. J. Antimicrob. Agents. 23 (2), 113–119. https://doi.org/10.1016/j.ijantimicag.2003.11.003.

Cafiso, V., Bertuccio, T., Spina, D., Purrello, S., Stefani, S., 2010. Tigecycline inhibition of a mature biofilm in clinical isolates of *Staphylococcus aureus*: comparison with other drugs. FEMS Immunol. Med. Microbiol. 59, 466–469. https://doi.org/10.1111/j.1574-695X.2010.00701.x.

Choudhary, A., Jain, P., Mohapatra, S., Mustafa, G., Ansari, M.J., Aldawsari, M.F., Alalaiwe, A,S., Mirza, M.A., Iqbal, Z., 2022. A novel approach of targeting linezolid nanoemulsion for the management of lymph node tuberculosis. ACS Omega. 25, 7 (18):15688-15694. https://doi.org/10.1021/acsomega.2c00592.

Clinical and Laboratory Standards Institute (CLSI), 2018. Methods for dilution antimicrobial susceptibility tests for bacteria that grow aerobically; Approved standard 11th ed.; M07; CLSI: Wayne, IL, USA.

Curtin, J., Cormican, M., Fleming, G., Keelehan, J., Colleran, E., 2003. Linezolid compared with eperezolid, vancomycin, and gentamicin in an in vitro model of antimicrobial lock therapy for *Staphylococcus epidermidis* central venous catheter-related biofilm infections. Antimicrob. Agents Chemother. 47, 3145–3148. https://doi.org/10.1128/AAC.47.10.3145-3148.2003.

Da Costa, D., Exbrayat-Héritier, C., Rambaud, B., Megy, S., Terreux, R., Verrier, B., Primard, C., 2021. Surface charge modulation of rifampicin-loaded PLA nanoparticles to improve antibiotic delivery in *Staphylococcus aureus* biofilms. J. Nanobiotechnol. 19, 12. https://doi.org/10.1186/s12951-020-00760-w.

Eren, Boncu, T., Uskudar, Guclu, A., Catma, M.F., Savaser, A., Gokce, A., Ozdemir, N., 2020. In vitro and in vivo evaluation of linezolid loaded electrospun PLGA and PLGA/PCL fiber mats for prophylaxis and treatment of MRSA induced prosthetic infections. Int. J. Pharm. 5, 573:118758. https://doi.org/10.1016/j.ijpharm.2019.118758.

Estes, K.S., Derendorf, H., 2010. Comparison of the pharmacokinetic properties of vancomycin, linezolid, tigecyclin, and daptomycin. Eur. J. Med. Res. 30,15(12): 533–43 https://doi.org/10.1186/2047-783x-15-12-533.

Fazio, E., Scala, A., Grimato, S., Ridolfo, A., Grassi, G., Neri, F., 2015. Laser light triggered smart release of silibinin from a PEGylated–PLGA gold nanocomposite. J. Mater. Chem. B. 3, 9023–9032. https://doi.org/10.1039/c5tb01076d.

Foti, C., Piperno, A., Scala, A., Giuffrè, O., 2021. Oxazolidinone antibiotics: chemical, biological and analytical aspects. Molecules. 26, 4280. https://doi.org/10.3390/molecules26144280.

Ghataty, D.S., Amer, R.I., Wasfi, R., Shamma, R.N., 2022. Novel linezolid loaded bio-composite films as dressings for effective wound healing: experimental design, development, optimization, and antimicrobial activity. Drug Deliv. 29, 3168–3185. https://doi.org/10.1080/10717544.2022.2127974.

Glinka, M., Filatova, K., Kucińska-Lipka, J., Bergerova, E.D., Wasik, A., Sedlařík, V., 2021. Encapsulation of Amikacin into Microparticles Based on Low-Molecular-Weight Poly(lactic acid) and Poly(lactic acid-co-polyethylene glycol). Mol. Pharm. 18, 2986–2996. https://doi.org/10.1021/acs.molpharmaceut.1c00193.

Guo, P., Buttaro, B.A., Xue, H.Y., Tran, N.T., Wong, H.L., 2020. Lipid-polymer hybrid nanoparticles carrying linezolid improve treatment of methicillin-resistant *Staphylococcus aureus* (MRSA) harbored inside bone cells and biofilms. Eur. J. Pharm. Biopharm. 151, 189–198. https://doi.org/10.1016/j.ejpb.2020.04.010.

Hada, A.M., Potara, M., Astilean, S., Cordaro, A., Neri, G., Malanga, M., Nostro, A., Mazzaglia, A., Scala, A., Piperno, A., 2022. Linezolid nanoAntiobiotics and SERS-nanoTags based on polymeric cyclodextrin bimetallic core-shell nanoarchitectures. Carbohyd. Polym. 293, 119736 https://doi.org/10.1016/j.carbpol.2022.119736.

Huang, J., Chen, Z., Li, Y., Li, L., Zhang, G., 2017. Rifapentine-linezolid-loaded PLGA microspheres for interventional therapy of cavitary pulmonary tuberculosis: preparation and in vitro characterization. Drug Des. Devel. Ther. 11, 585–592. https://doi.org/10.2147/DDDT.S127897.

Kalishwaralal, K., BarathManiKanth, S., Pandian, S.R., Deepak, V., Gurunathan, S., 2010. Silver nanoparticles impede the biofilm formation by *Pseudomonas aeruginosa* and *Staphylococcus epidermidis*. Colloids Surf. B Biointerfaces. 79, 340–344. https://doi:10.1016/j.colsurfb.2010.04.014.

Karlowsky, J.A., Hackel, M.A., Bouchillon, S.K., Alder, J., Sahm, D.F., 2017. In Vitro activities of Tedizolid and comparator antimicrobial agents against clinical isolates of *Staphylococcus aureus* collected in 12 countries from 2014 to 2016. Diagn. Microbiol. Infect. Dis. 89, 151–157. https://doi.org/10.1016/j.diagmicrobio.2017.07.001.

Labruère, R., Sona, A.J., Turos, E., 2019. Anti–methicillin-resistant *Staphylococcus aureus* nanoantibiotics. Front. Pharmacol. 10, 1121. https://doi.org/10.3389/fphar.2019.01121.

Liénard, R., Montesi, M., Panseri, S., Dozio, S.M., Vento, F., Mineo, P.G., Piperno, A., De Winter, J., Coulembier, O., Scala, A., 2020. Design of naturally inspired jellyfish-shaped cyclopolylactides to manage osteosarcoma cancer stem cells fate. Mater. Sci. Eng. C Mater. Biol. Appl. 117, 111291 https://doi.org/10.1016/j.msec.2020.111291.

Nostro, A., Marino, A., Blanco, A.R., Cellini, L., Di Giulio, M., Pizzimenti, F., Sudano Roccaro, A., Bisignano, G., 2009. In vitro activity of carvacrol against staphylococcal preformed biofilm by liquid and vapour contact. J. Med. Microbiol. 58, 791–797. https://doi.org/10.1099/jmm.0.009274-0. PMID: 19429756.

Nostro, A., Sudano Roccaro, A.S., Bisignano, G., Marino, A., Cannatelli, M.A., Pizzimenti, F.C., Cioni, P.L., Procopio, F., Blanco, A.R., 2007. Effects of oregano, carvacrol and thymol on *Staphylococcus aureus* and *Staphylococcus epidermidis* biofilms. J. Med. Microbiol. 56, 519–523 https://doi.og/10.1099/jmm.0.46804-0 PMID: 17374894.

Paczkowska-Walendowska, M., Rosiak, N., Tykarska, E., Michalska, K., Płazińska, A., Płaziński, W., Szymanowska, D., Cielecka-Piontek, J., 2021. Tedizolid-cyclodextrin system as delayed-release drug delivery with antibacterial activity. Int. J. Mol. Sci. 22, 115. https://doi.org/10.3390/ijms22010115.

Patil, K.D., Bagade, S.B., Bonde, S.C., 2020. In-vitro and ex-vivo characterization of novel mannosylated gelatin nanoparticles of linezolid by Quality-by-Design approach. J. Drug Deliv. Sci. Technol. 60, 101976 https://doi.org/10.1016/j.jddst.2020.101976.

Piperno, A., Sciortino, M.T., Giusto, E., Montesi, M., Panseri, S., Scala, A., 2021. Recent advances and challenges in gene delivery mediated by polyester-based nanoparticles. Int. J. Nanomedicine. 31 (16), 5981–6002. https://doi.org/10.2147/IJN.S321329.

Scaffaro, R., Lopresti, F., Marino, A., Nostro, A., 2018. Antimicrobial additives for poly (lactic acid) materials and their applications: current state and perspectives. Appl. Microbiol. Biotechnol. 102, 7739–7756. Erratum. In: 10.1007/s00253-018-9251-7.

Scala, A., Piperno, A., Micale, N., Mineo, P.G., Abbadessa, A., Risoluti, R., Castelli, G., Bruno, F., Vitale, F., Cascio, C., Grassi, G., 2018a. "Click" on PLGA-PEG and hyaluronic acid: gaining access to anti-leishmanial pentamidine bioconjugates. J. Biomed. Mater. Res. Part B. 106, 2778–2785. https://doi.org/10.1002/jbm.b.34058.

Scala, A., Piperno, A., Torcasio, S.M., Nicosia, A., Mineo, P.G., Grassi, G., 2018b. "Clickable" polylactic acids obtained by solvent free intra-chain amidation. Eur. Polymer. J. 109, 341–346. https://doi.org/10.1016/j.eurpolymj.2018.10.004.

Shah, S., Maheshwari, H., Soniwala, M., Chavda, J., 2022. Pulmonary delivery of linezolid nanoparticles for treatment of tuberculosis: design, development, and optimization. J. Pharm. Innov. 17, 46–59. https://doi.org/10.1007/s12247-020-09491-9.

Sivori, F., Cavallo, I., Kovacs, D., Guembe, M., Sperduti, I., Truglio, M., Pasqua, M., Prignano, G., Mastrofrancesco, A., Toma, L., Pimpinelli, F., Morrone, A., Ensoli, F., Di Domenico, E.G., 2022. Role of extracellular DNA in dalbavancin activity against methicillin-resistant *Staphylococcus aureus* (MRSA) biofilms in patients with skin and soft tissue infections. Microbiol. Spectr. 10, e0035122.

Tammaro, L., Saturnino, C., D'Aniello, S., Vigliotta, G., Vittoria, V., 2015. Polymorphic solidification of Linezolid confined in electrospun PCL fibers for controlled release in topical applications. Int. J. Pharm. 490, 32–38. https://doi.org/10.1016/j.ijpharm.2015.04.070.

Torcasio, S.M., Oliva, R., Montesi, M., Panseri, S., Bassi, G., Mazzaglia, A., Piperno, A., Coulembier, O., Scala, A., 2022. Three-armed RGD-decorated starPLA-PEG nanoshuttle for docetaxel delivery. Biomater. Adv. 140, 213043 https://doi.org/10.1016/j.bioadv.2022.213043.

Tyler, B., Gullotti, D., Mangraviti, A., Utsuki, T., Brem, H., 2016. Polylactic acid (PLA) controlled delivery carriers for biomedical applications. Adv. Drug Delivery Rev. 107, 163–175. https://doi.org/10.1016/j.addr.2016.06.018.